



Simulation of Turbulent Plane Channel Flow Using Fourier Pseudo-Spectral and Immersed Boundary Methods with Spalart-Allmaras Turbulence Modeling

Laura A. V. Albuquerque¹, Mariana F. S. Villela¹, Felipe P. Mariano²

¹Computational Engineering Group, Federal University of Pernambuco (UFPE)

Av. Marielle Franco, KM59, s/n, Nova Caruaru, 55014-900, Pernambuco, Brazil

laura.vasconcelos@ufpe.br, mariana.villela@ufpe.br

²Laboratory of Thermal and Fluid Engineering (LATEF), Federal University of Goiás (UFG)

Av. Esperança, Al. Ingá, Prédio: B5, Campus Samambaia, 74690-900, Goiás, Brazil

fpmariano@ufg.br

Abstract. This study presents a novel approach that integrates the Spalart-Allmaras turbulence model with the Fourier pseudo-spectral method to simulate turbulent channel flow. The methodology is particularly suited for capturing the nuances of turbulence within channel flows, offering a balance between computational efficiency and accuracy. The proposed approach was validated against high-fidelity DNS data from Lee and Monser [1], corresponding to a Reynolds number of $Re = 40,000$ or $Re_\tau = 1,000$. The results demonstrate a strong correlation between the simulated outcomes and DNS data, particularly in accurately reproducing the mean velocity profiles and viscous shear stress distributions. This validation underscores the effectiveness of the combined methodology in turbulent flow simulations, suggesting its potential for broader applications in engineering and fluid dynamics research.

Keywords: Turbulent Channel Flow, Spalart-Allmaras Turbulence Model, Fourier Pseudo-Spectral Method

1 Introduction

Most practical applications of fluid mechanics involve turbulent flows, characterized by their instability and fluctuations that depend on both time and spatial position. Turbulent flows near the Earth's surface, where roughness is exceptionally variable, are particularly important for predicting the potential and sizing of wind generators and wind farms [2]. One of the key challenges in studying turbulent flows is the multiplicity of scales that characterize them. The largest structures (low frequencies) are controlled by the geometry that generates them, while the smallest structures (high frequencies) are governed by the fluid's viscosity. The turbulent regime is predominant because small perturbations are naturally amplified, leading to instabilities and transition [3].

The Navier-Stokes equations, coupled with the continuity equation, are fundamental in modeling both laminar and turbulent flows. However, at high Reynolds numbers (Re), Direct Numerical Simulation (DNS) becomes infeasible due to the substantial computational cost required to resolve the full energy spectrum, with the number of degrees of freedom scaling as $Re^{9/4}$ [4]. This results in an extremely large linear system that must be solved, which is proportional to the degrees of freedom of the turbulent flow [5]. To address this, researchers have developed various turbulence closure models that filter the balance equations, resulting in the emergence of new terms that require modeling.

Among the methodologies developed to model and simulate turbulent flows, Unsteady Reynolds-Averaged Navier-Stokes Equations (URANS) and Large Eddy Simulation (LES) are commonly used. LES resolves large scales while modeling only the smaller scales, making it suitable for high-resolution simulations. URANS, the focus of this study, employs a non-permanent filtered field to model turbulent flows, offering a balance between computational cost and accuracy [3]. This makes URANS particularly useful for engineering applications where fully resolved simulations like DNS are not feasible.

In addition to turbulence modeling, another significant challenge in computational fluid dynamics (CFD) is the need for efficient computational tools, particularly when dealing with complex geometries in real-world turbulent flows. The Immersed Boundary Method (IBM) offers an efficient solution by using body-unfitted grids, simplifying mesh generation and allowing for it to be performed once at the start of a simulation [6]. IBM's

ability to fully immerse solid boundaries within the computational grid enables more flexible handling of complex geometries without the need for mesh refinement.

High-accuracy computer simulations can be achieved by solving fluid flow equations using high-order numerical methods such as spectral methods, which are known for their exponential convergence rate with mesh refinement. The collocation Fourier pseudo-spectral method (FPSM) is particularly effective for solving the Navier-Stokes equations, as it eliminates the need for solving the pressure gradient in incompressible flows by ensuring mass conservation through the projection of the nonlinear term [7]. This method replaces the solution of the Poisson equation with a matrix-vector product, which is computationally faster and requires less RAM. The pressure field can still be obtained during post-processing. The main computational cost of using FPSM lies in transforming the velocity fields into spectral space. This is done using the fast Fourier transform (FFT) algorithm, which is often more efficient than solving linear systems, particularly in simulations with a finer mesh refinement [7]. However, the FPSM requires periodic boundary conditions, limiting its applicability in CFD to a few specific problems.

The integration of immersed boundary and Fourier pseudo-spectral methods forms the approach known as IMERSPEC, as outlined in Mariano et al. [7] and Nascimento et al. [8]. This methodology aims to leverage the strengths of both techniques while addressing certain limitations. To circumvent the necessity of periodic boundary conditions when employing FFT, Mariano et al. [7] suggest partitioning the computational domain into two sections using IBM. Within the physical domain, boundary conditions are enforced via IBM, while externally, the complementary domain applies the periodic boundary conditions essential for FFT computations.

Building on this foundation, the present study extends the IMERSPEC methodology to simulate turbulent flow using the Reynolds-averaged Navier-Stokes equations and the Spalart-Allmaras turbulence model [9]. By validating the numerical results against DNS data for a flat channel flow at $Re = 40,000$, we aim to assess the effectiveness and accuracy of this combined approach in capturing the key characteristics of turbulent flows. This study contributes to the ongoing development of efficient and accurate CFD methods, with potential applications in aerodynamic and fluid dynamic engineering studies.

2 Mathematical Modeling and Numerical Method

Turbulent isothermal flows of Newtonian fluids can be described using the continuity and Navier-Stokes equations. When dealing with incompressible flows, these equations, subjected to the mean temporal operator, are expressed as Eq. 1 and Eq. 2, utilizing indicial notation:

$$\frac{\partial(\bar{u}_i)}{\partial x_i} = 0, \quad (1)$$

$$\frac{\partial \bar{u}_i}{\partial t} + \frac{\partial}{\partial x_j} (\bar{u}_i \bar{u}_j) = -\frac{1}{\rho} \frac{\partial \bar{p}}{\partial x_i} + \frac{\partial}{\partial x_j} \left[\nu \left(\frac{\partial \bar{u}_i}{\partial x_j} + \frac{\partial \bar{u}_j}{\partial x_i} \right) - \overline{u'_i u'_j} \right] + \frac{\bar{f}_i}{\rho}, \quad (2)$$

where \bar{p} is the mean pressure [N/m^2]; \bar{u}_i is the mean velocity in the i -direction [m/s]; \bar{f}_i is a source term [N/m^3]; ρ is the density [kg/m^3]; ν is the kinematic viscosity [m^2/s]; x_i is the spatial coordinate (x or y) [m]; and t is the time [s].

It is important to note that Eq. 2 includes an additional term $\overline{u'_i u'_j}$, known as the Reynolds stress tensor, which remains unknown. This term renders the model mathematically open, necessitating the inclusion of an additional equation for model closure. Boussinesq proposed to model this tensor using his hypothesis, which involves making an analogy to the Stokes model for the molecular viscous stress tensor [3]. The model is represented by Eq. 3.

$$-\overline{u'_i u'_j} = \nu_t \left(\frac{\partial \bar{u}_i}{\partial x_j} + \frac{\partial \bar{u}_j}{\partial x_i} \right) + \frac{2}{3} k \delta_{ij}, \quad (3)$$

where $k = \frac{1}{2} \overline{u'_i u'_i}$ denotes turbulent kinetic energy, δ_{ij} is the Kronecker delta, and ν_t is the kinematic turbulent viscosity. Unlike molecular viscosity, which is inherent to fluids, turbulent viscosity is a property of the flow.

Turbulent viscosity ν_t can be calculated using a turbulence model such as the Spalart-Allmaras, as employed in the present study. The turbulent kinetic energy is incorporated into the pressure term, generating a modified pressure p^* . With these considerations, we can express Eq. 2 as follows:

$$\frac{\partial \bar{u}_i}{\partial t} + \frac{\partial}{\partial x_j} (\bar{u}_i \bar{u}_j) = -\frac{1}{\rho} \frac{\partial p^*}{\partial x_i} + \frac{\partial}{\partial x_j} \left[(\nu + \nu_t) \left(\frac{\partial \bar{u}_i}{\partial x_j} + \frac{\partial \bar{u}_j}{\partial x_i} \right) \right] + \frac{\bar{f}_i}{\rho}. \quad (4)$$

2.1 The Spalart-Allmaras Turbulence Model

The Spalart-Allmaras (SA) turbulence model was developed and calibrated based on empirical relationships from various flow types and dimensional analysis [3]. This model is grounded in a transport equation for the auxiliary variable $\tilde{\nu}$, as depicted in Eq. 5, disregarding transition terms. These terms, typically negligible in fully developed turbulent flows, are omitted in the case under study.

$$\frac{\partial \tilde{\nu}}{\partial t} + \frac{\partial}{\partial x_j} (u_j \tilde{\nu}) = C_{b1} \tilde{S} \tilde{\nu} - C_{w1} f_w \left(\frac{\tilde{\nu}}{d} \right)^2 + \frac{1}{\sigma} \left[\frac{\partial}{\partial x_j} \left((\nu + \tilde{\nu}) \frac{\partial \tilde{\nu}}{\partial x_j} \right) + C_{b2} \frac{\partial \tilde{\nu}}{\partial x_j} \frac{\partial \tilde{\nu}}{\partial x_j} \right]. \quad (5)$$

The terms on the right-hand side of Eq. 5 represent, respectively, the production, destruction, molecular and turbulent diffusion, and dissipation of viscosity. The d is the distance to the nearest wall. The turbulent viscosity ν_t is defined through the modified viscosity $\tilde{\nu}$ and is damped by the function f_1 near the walls:

$$\nu_t = \tilde{\nu} f_{\nu_1}, \quad f_{\nu_1} = \frac{\chi^3}{\chi^3 + C_{\nu_1}^3}, \quad \text{where } \chi = \frac{\tilde{\nu}}{\nu}. \quad (6)$$

In regions distant from the wall, the damping function f_1 tends towards unity, $\nu_t = \tilde{\nu}$. The production term varies with the distance from the wall and is attenuated by the function f_{ν_2} :

$$\tilde{S} = S + \frac{\tilde{\nu}}{\kappa^2 d^2} f_{\nu_2} \quad \text{where } f_{\nu_2} = 1 - \frac{\chi}{1 + \chi f_{\nu_1}}. \quad (7)$$

In Eq. 7, the mean rate of flow deformation, S , is defined in terms of the magnitude of the vorticity tensor, Ω :

$$S = \sqrt{2\Omega_{ij}\Omega_{ij}}, \quad \Omega_{ij} = \frac{1}{2} \left(\frac{\partial u_i}{\partial x_j} - \frac{\partial u_j}{\partial x_i} \right). \quad (8)$$

The function f_w is defined as unity within the logarithmic region of the boundary layer, enhancing the production term as it approaches the wall and approaching zero for regions farther away. Its definition is:

$$f_w = g \left[\left(1 + \frac{C_{w3}^6}{g^6 + C_{w3}^6} \right)^{\frac{1}{6}} \right], \quad g = r + C_{w2}(r^6 - r), \quad r = \frac{\tilde{\nu}}{\bar{S}\kappa^2 d^2}. \quad (9)$$

The remaining empirical constants of the model are shown in Eq. 10. The number of variables in the model makes it evident that it was designed based on well-known flows, particularly turbulent boundary layers.

$$C_{w1} = \frac{C_{b1}}{\kappa^2} + \frac{1 + C_{b2}}{\sigma}, \quad C_{w2} = 0.3, \quad C_{w3} = 2, \quad \kappa = 0.41, \quad C_{\nu_1} = 7.1, \quad \sigma = \frac{2}{3}, \quad (10)$$

$$C_{b1} = 0.1355, \quad C_{b2} = 0.622, \quad C_{t1} = 1, \quad C_{t2} = 2, \quad C_{t3} = 1.1, \quad C_{t4} = 2.$$

2.2 Immersed boundary method – IBM

The Immersed Boundary Method utilizes two calculation domains: the Eulerian and Lagrangian domains. In the Eulerian domain, fluid flow equations are solved, while the force field is assessed in the Lagrangian domain to represent the immersed interface of the flow [7]. These domains interact via a source term added to the Navier–Stokes equations, as shown in Eq. 4. This source term is defined across the entirety of the Eulerian domain, considering its distribution over the Lagrangian domain, as outlined in Eq. 11.

$$f_i(\vec{x}, t) = \begin{cases} F_i(\vec{X}, t) & \text{if } \vec{x} = \vec{X}. \\ 0 & \text{if } \vec{x} \neq \vec{X}. \end{cases} \quad (11)$$

The position of a fluid particle is denoted by \vec{x} , while \vec{X} represents the position of a fluid particle adjacent to the solid interface, as depicted in Fig. 1. The source term has non-zero values only at points coinciding with the immersed geometry. This allows the Eulerian field to detect the presence of a solid interface [10].

The Multi-Direct Forcing (MDF) method proposed by Wang et al. [11] is the immersed boundary method applied in the present work. The interface force is calculated iteratively using MDF to improve the accuracy of the Lagrangian force calculation, $F_i(\vec{X}, t)$. MDF aims to enforce the desired value of certain properties at the body boundary [7]. $F_i(\vec{X}, t)$ is determined through momentum equations applied to fluid particles residing at the fluid–solid interface, as illustrated in Equation 12. The capital symbols are the same as Eq. 4, but they are calculated only over the Lagrangian interface (Γ) shown in Fig. 1.

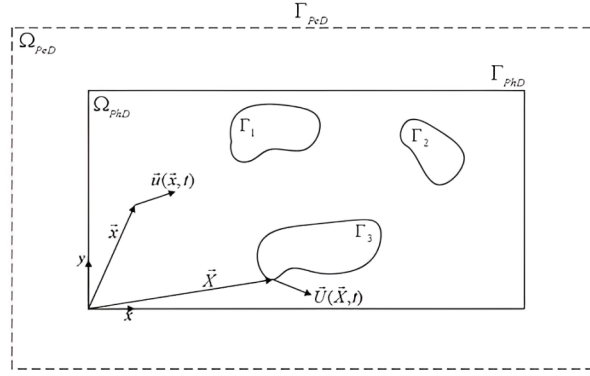


Figure 1. Schematic representation of the Eulerian and Lagrangian domains

$$F_i(\vec{X}, t) = \frac{\partial \bar{U}_i}{\partial t}(\vec{X}, t) + \frac{\partial}{\partial X_j} (\bar{U}_i \bar{U}_j)(\vec{X}, t) + \frac{1}{\rho} \frac{\partial \bar{P}^*}{\partial X_i}(\vec{X}, t) - \frac{\partial}{\partial X_j} \left[(\nu + \nu_t) \left(\frac{\partial \bar{U}_i}{\partial X_j} + \frac{\partial \bar{U}_j}{\partial X_i} \right) \right]. \quad (12)$$

By employing the temporal parameter U^* proposed by Wang et al. [11] and discretizing the time operator, we obtain Eq. 13 [7]. It is important to highlight that the time derivative in this equation was discretized using the explicit Euler method, chosen for explanatory and didactic purposes to aid in understanding the modeling. In the present work, temporal discretization was performed using the fourth-order Runge–Kutta method.

$$F_i(\vec{X}, t) = \frac{U_i(\vec{X}, t + \Delta t) - U_i^*(\vec{X}, t) + U_i^*(\vec{X}, t) - U_i(\vec{X}, t)}{\Delta t} + RHS_i(\vec{X}, t). \quad (13)$$

where Δt is the timestep and,

$$RHS_i(\vec{X}, t) = \frac{\partial}{\partial X_j} (\bar{U}_i \bar{U}_j)(\vec{X}, t) + \frac{1}{\rho} \frac{\partial \bar{P}^*}{\partial X_i}(\vec{X}, t) - \frac{\partial}{\partial X_j} \left[(\nu + \nu_t) \left(\frac{\partial \bar{U}_i}{\partial X_j} + \frac{\partial \bar{U}_j}{\partial X_i} \right) \right]. \quad (14)$$

Equation 13 is solved by decomposition, resulting in Eqs. 15 and 16:

$$\frac{U_i^*(\vec{X}, t) - U_i(\vec{X}, t)}{\Delta t} + RHS_i(\vec{X}, t) = 0, \quad (15)$$

$$F_i(\vec{X}, t) = \frac{U_i(\vec{X}, t + \Delta t) - U_i^*(\vec{X}, t)}{\Delta t}. \quad (16)$$

where $U_i(\vec{X}, t + \Delta t) = U_{FI}$ is the immersed boundary velocity, and $U_i^*(\vec{X}, t)$ is given by:

$$U_i(\vec{X}, t) = \begin{cases} u_i^*(\vec{x}, t) & \text{if } \vec{x} = \vec{X}. \\ 0 & \text{if } \vec{x} \neq \vec{X}. \end{cases} \quad (17)$$

Equation 15 is solved in the Eulerian domain using the Fourier spectral space. The term $u_i^*(\vec{x}, t)$ is then interpolated to the Lagrangian domain, resulting in $U_i^*(\vec{X}, t)$, as computed in Eq. 16. This result is then mapped back to the Eulerian collocation points. Finally, the Eulerian velocities are updated using Eq. 18.

$$u_i(\vec{x}, t + \Delta t) = u_i^*(\vec{x}, t) + \Delta t f_i. \quad (18)$$

2.3 Fourier Pseudo-Spectral Method – FPSM

Equations 1 and 2 in the Fourier space are given by Eqs. 19 and 20:

$$\frac{\partial \widehat{u}_j}{\partial x_j} = ik_j \widehat{u}_j = 0, \quad (19)$$

$$\frac{\widehat{\partial \bar{u}_i}}{\partial t} = -\frac{\partial}{\partial x_j} (\bar{u}_i \bar{u}_j) - \frac{1}{\rho} \frac{\partial \widehat{p}^*}{\partial x_i} + \frac{\partial}{\partial x_j} \left[\nu_{ef} \left(\frac{\partial \bar{u}_i}{\partial x_j} + \frac{\partial \bar{u}_j}{\partial x_i} \right) \right] + \frac{\widehat{f}_i}{\rho}. \quad (20)$$

where k_j and \hat{u}_j are the wave vector and the transformed velocity vector, respectively, and $\nu_{ef} = \nu + \nu_t$.

Equation 19 illustrates the orthogonality between the wave number vector k_i and the transformed velocity $\hat{u}_i(\vec{k}, t)$. We introduce the concept of a divergence-free vector plane, denoted as the π -plane. This plane is orthogonal to the wave number vector, implying that the transformed velocity resides within it. In the establishment of this plane, each component in Eq. 20 assumes a distinct spatial orientation: the transient term and the viscous term are contained within the plane, whereas the pressure gradient term is perpendicular to it. The orientation of the nonlinear term is initially undetermined. Upon combining the components of Eq. 20, we find that:

$$\underbrace{\left(\frac{\partial \widehat{u}_i}{\partial t} \right)}_{\in \pi} + \underbrace{\left(\frac{\partial (\bar{u}_i \bar{u}_j)}{\partial x_j} + ik_i \widehat{p}^* - \frac{\partial}{\partial x_j} \left[\nu_{ef} \left(\frac{\partial \bar{u}_i}{\partial x_j} + \frac{\partial \bar{u}_j}{\partial x_i} \right) \right] + \frac{\widehat{f}_i}{\rho} \right)}_{\in \pi} = 0. \quad (21)$$

Equation 21 implies that:

$$\frac{\partial (\bar{u}_i \bar{u}_j)}{\partial x_j} + ik_i \widehat{p}^* - \frac{\partial}{\partial x_j} \left[\nu_{ef} \left(\frac{\partial \bar{u}_i}{\partial x_j} + \frac{\partial \bar{u}_j}{\partial x_i} \right) \right] + \frac{\widehat{f}_i}{\rho} = \varphi_{im} \left[\frac{\partial (\bar{u}_m \bar{u}_j)}{\partial x_j} - \frac{\partial}{\partial x_j} \left[\nu_{ef} \left(\frac{\partial \bar{u}_m}{\partial x_j} + \frac{\partial \bar{u}_j}{\partial x_m} \right) \right] + \frac{\widehat{f}_i}{\rho} \right], \quad (22)$$

where φ_{im} is the projection tensor. The gradient pressure field is orthogonal to the π -plane. Consequently, the pressure and velocity fields in Fourier space are no longer coupled. Nonetheless, the pressure field can be recovered through a post-processing procedure, as demonstrated by Mariano et al. [7].

The non-linear term yields a product of transformed functions, which, according to the properties of Fourier transforms, translates into a convolution operation and its solution is represented by a convolution integral. Solving this integral computationally is highly expensive. Thus, it is managed through the pseudo-spectral Fourier method. As a result, the momentum equation in Fourier space, employing the projection method, takes the following form:

$$\frac{\widehat{\partial \bar{u}_i}(\vec{k}, t)}{\partial t} = -ik_j \varphi_{im} \int_{\vec{k}=\vec{r}+\vec{s}} \widehat{u}_m(\vec{r}) \widehat{u}_j(\vec{k}-\vec{r}) d\vec{r} + ik_j \varphi_{im} \int_{\vec{k}=\vec{r}+\vec{s}} \widehat{\nu}_{ef}(\vec{r}) \left(\frac{\partial \bar{u}_m}{\partial x_j} + \frac{\partial \bar{u}_j}{\partial x_m} \right) (\vec{k}-\vec{r}) d\vec{r}. \quad (23)$$

The non-linear term can be handled in different forms. The skew-symmetric is more stable and presents better results [8]. Therefore, this procedure is used in this study. The non-linear term is solved using the pseudo-spectral method. The velocity product is calculated in physical space and then transformed to spectral space.

3 Methodology

The simulation of fully developed flow in a channel is widely utilized to validate turbulence models due to the simplicity of its geometry, making it particularly suitable for turbulence studies. Numerous researchers have conducted accurate DNS calculations. In this work, data from Lee and Monser [1] is utilized as a reference.

The proposed numerical methodology combines the Spalart-Allmaras turbulence model and the Fourier pseudo-spectral method to simulate turbulent channel flow. This methodology was validated at a Reynolds number of $Re = 40,000$ or $Re_\tau = \frac{u_\tau h}{\nu} = 1,000$, where u_τ denotes the friction velocity and h represents half the channel height. The no-slip boundary condition was applied in the normal direction to the wall, while the symmetry condition was applied in the spanwise direction. In the streamwise direction, periodic boundary conditions were imposed using the immersed boundary method. The computational domain is structured with dimensions $L_x = 10h$ and $L_y = h$, discretized using a uniform grid of 64×128 collocation points in the spanwise direction.

The proposed algorithm proceeds through several sequential steps: initially, solving Eq. 22 in Fourier spectral space to compute the temporal parameter $\widehat{u}_i(\vec{k}, t)$ using the 4-step Runge-Kutta method. Subsequently, applying an Inverse Fast Fourier Transform to $\widehat{u}_i(\vec{k}, t)$ yields $\bar{u}_i(\vec{x}, t)$ in physical space. This transformed field $\bar{u}_i(\vec{x}, t)$ is then interpolated into the Lagrangian domain using Eq. 17. Concurrently, the Lagrangian force $F_i^*(\vec{X}, t)$ is computed according to Eq. 16, and the Eulerian force $f_i^*(\vec{x}, t)$ is derived using Eq. 17. The algorithm then updates the Eulerian velocity to $u_i(\vec{x}, t + \Delta t)$ with Eq. 18, transforms it back to spectral space using FFT to obtain $\hat{u}_i(\vec{k}, t + \Delta t)$, and cycles back to the initial step for iterative repetition.

4 Results

The flow exhibits statistical homogeneity in the mean-flow and spanwise directions, facilitating Fourier representations with N_x and N_y modes, respectively. In physical space, grid nodes are uniformly spaced with $\Delta x = L_x/N_x$ and $\Delta y = L_y/N_y$ in the x and y directions. Figure 2 compares the mean velocity profiles, normalized by centerline velocity and plotted as a function of distance across the channel (normalized by channel width), for fully developed flow with DNS data. Figure 3 shows the profile of the viscous shear stress, also compared with DNS data.

From the analysis of these figures, it can be concluded that the numerical results align well with the DNS data. The mean velocity profile, as shown in Fig. 2, closely follows the trend of the DNS data across the channel, indicating that the proposed methodology accurately captures the velocity distribution. The maximum absolute difference between the obtained result and the reference was 2.011%. Similarly, the viscous shear stress profile in Fig. 3 demonstrates a good match with the DNS results, reflecting the algorithm's capability to reproduce the stress distribution within the channel flow.

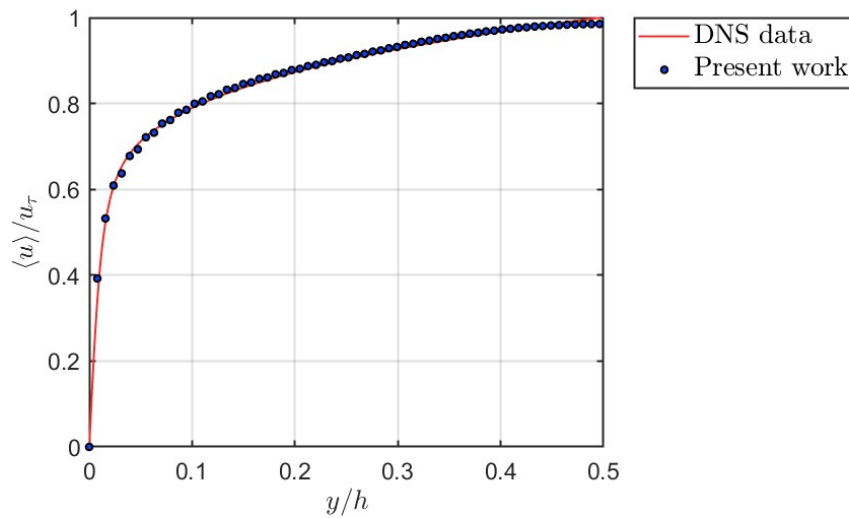


Figure 2. Mean velocity profiles in fully developed turbulent channel flow

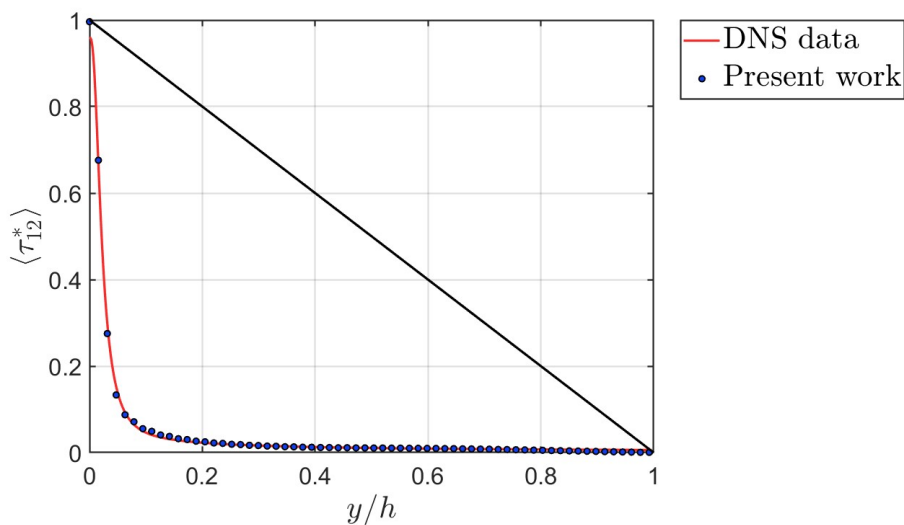


Figure 3. Comparison of viscous shear stress profiles between DNS data and present work

These comparisons validate the effectiveness of the combined Spalart-Allmaras turbulence model and Fourier

pseudo-spectral method in simulating turbulent channel flow, thereby providing a reliable tool for further turbulence studies.

5 Conclusions

The integration of the IMERSPEC method with the Spalart-Allmaras turbulence model has demonstrated a high level of effectiveness in simulating turbulent flows in a plane channel. The results obtained in this study, particularly the mean velocity and shear stress profiles, exhibit strong agreement with DNS data, validating the accuracy and reliability of the proposed approach. This confirms the potential of the IMERSPEC methodology in providing realistic and statistically efficient flow simulations.

Given the promising results, the methodology is recommended for more complex turbulent flow simulations, especially in scenarios involving intricate geometries or higher Reynolds numbers. Future research could explore the application of this combined approach in aerodynamic studies or environmental fluid dynamics, where accurate turbulence modeling is crucial.

Acknowledgements. The authors wish to acknowledge the financial support received from FURNAS Centrais Elétricas and the “Programa de Pesquisa e Desenvolvimento Tecnológico” (P&D) of ANEEL.

Authorship statement. The authors hereby confirm that they are the sole liable persons responsible for the authorship of this work, and that all material that has been herein included as part of the present paper is either the property (and authorship) of the authors, or has the permission of the owners to be included here.

References

- [1] M. Lee and R. D. Moser. Direct numerical simulation of turbulent channel flow up to $Re_\tau = 5200$. *Journal of Fluid Mechanics*, vol. 774, pp. 395–415, 2015.
- [2] C. Grinderslev, N. N. Sørensen, S. G. Horcas, N. Troldborg, and F. Zahle. Wind turbines in atmospheric flow: fluid–structure interaction simulations with hybrid turbulence modeling. *Wind Energy Science*, vol. 6, n. 3, pp. 627–643, 2021.
- [3] A. Silveira-Neto. *Escoamentos Turbulentos: Análise Física e Modelagem Teórica*. Composer, Uberlândia, 2020.
- [4] S. B. Pope. *Turbulent Flows*. Cornell University, New York, 2000.
- [5] G. M. Magalhães. *Modelagem matemática e computacional de escoamentos turbulentos multifásicos em malha adaptativa bloco estruturada utilizando método Multi Direct Forcing*. PhD thesis, Universidade Federal de Uberlândia, 2022.
- [6] F. Liao and X. Yang. On the capability of the curvilinear immersed boundary method in predicting near-wall turbulence of turbulent channel flows. *Theoretical and Applied Mechanics Letters*, vol. 11, n. 4, pp. 100279, 2021.
- [7] F. P. Mariano, L. Q. Moreira, A. A. Nascimento, and A. Silveira-Neto. An improved immersed boundary method by coupling of the multi-direct forcing and fourier pseudo-spectral methods. *Journal of the Brazilian Society of Mechanical Sciences and Engineering*, , n. 44, pp. 388, 2022.
- [8] A. A. Nascimento, F. P. Mariano, A. Silveira-Neto, and E. L. M. Padilla. Coupling of the immersed boundary and fourier pseudo-spectral methods applied to solve fluid–structure interaction problems. *Journal of the Brazilian Society of Mechanical Sciences and Engineering*, , n. 46, pp. 213, 2024.
- [9] P. R. Spalart and S. R. Allmaras. A one-equation turbulence model for aerodynamic flows. *Recherche Aerospaciale*, , n. 1, pp. 5–21, 1994.
- [10] L. Q. Moreira, A. Silveira-Neto, and F. P. Mariano. Application of a fourier spectral method to a non-periodic free shear flow. *21st International Congress of Mechanical Engineering, COBEM*, 2011.
- [11] Z. Wang, J. Fan, and K. Luo. Combined multi-direct forcing and immersed boundary method for simulating flows with moving particles. *International Journal of Multiphase Flow*, vol. 34, n. 3, pp. 283–302, 2008.